International Journal of Nanomedicine

Dovepress
Taylor & Francis Group

Open Access Full Text Article

ORIGINAL RESEARCH

3D-Printed Poly (Lactic-Co-Glycolic Acid) and Graphene Oxide Nerve Guidance Conduit with Mesenchymal Stem Cells for Effective Axon Regeneration in a Rat Sciatic Nerve Defect Model

Meaghan E Harley-Troxell[1], Alisha P Pedersen[1], Steven D Newby[1], Eli Christoph[1], Stacy Stephenson[2], Thomas J Masi[3], Dustin L Crouch[4], David E Anderson[1], Madhu Dhar[1]

[1]Tissue Engineering and Regenerative Medicine Laboratory, Large Animal Clinical Sciences, College of Veterinary Medicine, University of Tennessee, Knoxville, TN, 37996, USA; [2]Plastic and Reconstructive Surgery, University of Tennessee Medical Center, Knoxville, TN, 37920, USA; [3]Department of Surgery, University of Tennessee Graduate School of Medicine, Knoxville, TN, 37996, USA; [4]Mechanical, Aerospace, and Biomedical Engineering, University of Tennessee, Knoxville, TN, 37996, USA

Correspondence: Madhu Dhar, University of Tennessee, 2407 River Drive, Knoxville, TN, 37996, USA, Tel +1 865 974 8387, Email mdhar@utk.edu

Introduction: Peripheral nerve injuries (PNIs) impact the quality of life of millions of people. The current gold standard of treatment, the autograft, fails to restore nerve function and is often associated with untoward effects. The alternative interventions available remain unable to ensure full functional recovery. For this study we developed a 3D printed nerve guidance conduit (NGC) composed of poly (lactic-co-glycolic acid) (PLGA) and 0.25% graphene oxide (GO), that can be seeded with human adipose-derived mesenchymal stem cells (MSCs), to develop a more effective treatment for PNI.

Methods: We evaluated material degradation, surface topography, and MSC attachment in vitro. For the in vivo analyses, a 10-mm long sciatic nerve defect model was created, and rats were randomly divided into 4 treatment groups: autograft, PLGA, PLGA/GO, and PLGA/GO with 1×10^6 MSCs. For a 6-month period: biomechanics were evaluated using a pressure mat walkway to determine functional repair; systemic toxicity was evaluated using transmission electron microscopy of kidney and lung tissue; immunohistochemistry evaluated local adverse effects, myelin sheath and axonal repair; and gross muscle analyses of the lateral gastrocnemius, medial gastrocnemius, and soleus evaluated muscle reinnervation.

Results: In vitro results showed expected degradation rates, and the addition of GO exhibited cytocompatibility and favorable cell attachment. In vivo results showed biocompatibility with no translocation of the graphene nanoparticles. Histology showed evidence of axonal and myelin sheath repair. Biomechanics and gross muscle analyses had contradicting evidence of functional repair with the addition of GO. No differences were seen with the addition of MSCs.

Conclusion: Our novel PLGA/GO NGC, both with and without MSCs, showed results comparable to or greater than the current gold standard, as well as ease of use surgically. With further studies to validate functional recovery, this specific combination of PLGA and GO may provide an effective biomimetic therapy to repair PNIs.

Keywords: carbon-based nanoparticles, tissue engineering, nerve conduit, 3D printing

Introduction

Peripheral nerve injuries (PNI) affect an estimated 20 million people in the United States (US) alone.[1,2] PNIs account for 3% of all trauma patients, and most are caused by trauma resulting in lacerating, penetrating, traction, and crush injuries.[3] Less protected than the central nervous system, peripheral nerves are more easily damaged, yet maintain the ability to self-repair post-injury.[4,5] However, the successful outcome of this repair depends heavily on the site, severity, and type of injury, which are further complicated by ongoing Wallerian degeneration, slow nerve growth (1–3 mm/day), and retraction of disconnected tissue.[6,7] For these reasons, 33% of PNIs result in complete loss or only partial recovery of motor, sensory, and

Received: 16 October 2024
Accepted: 24 February 2025
Published: 13 March 2025

Graphical Abstract

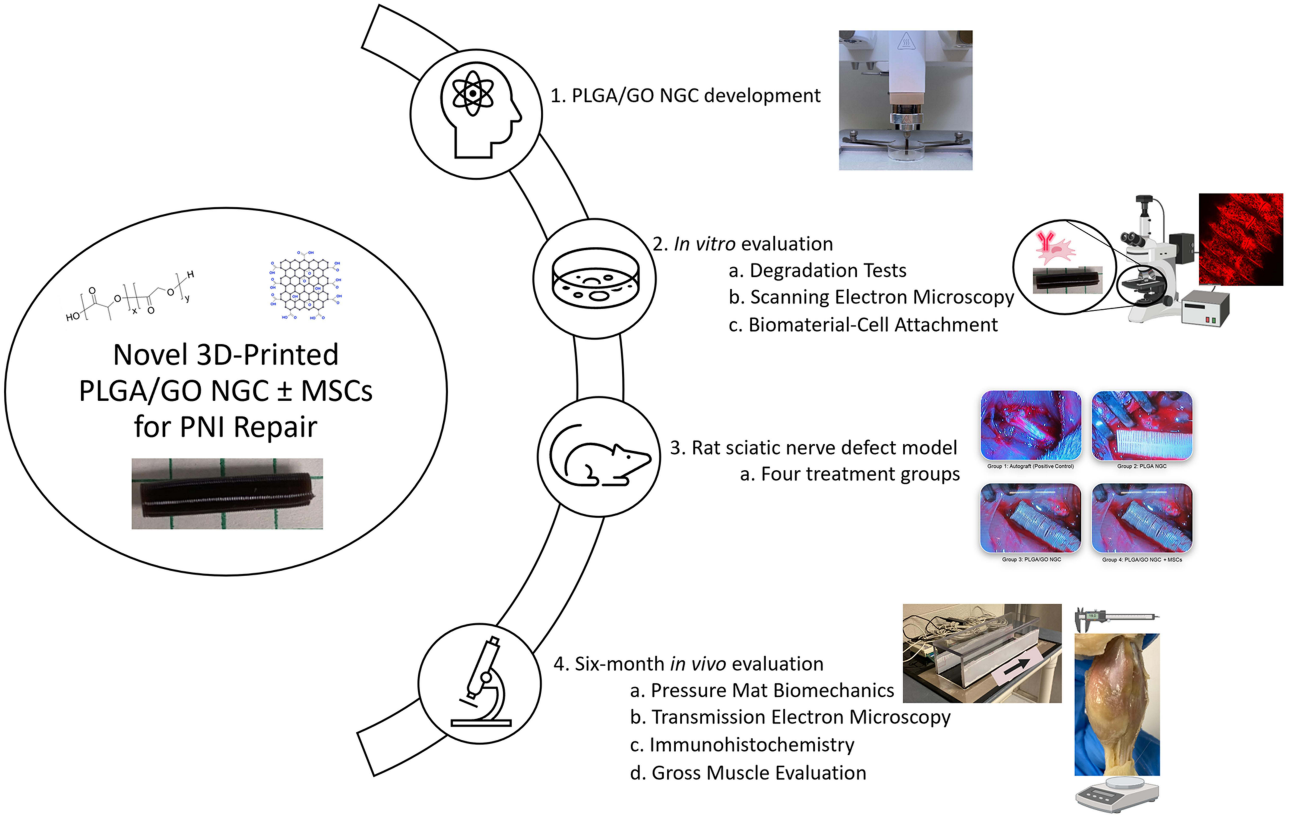

autonomic functions, and can be associated with chronic pain, muscle atrophy and weakness.[8] There are a range of surgical and non-surgical treatments available, but the functional outcome often leaves patients permanently disabled.[4,7] For nerve gaps larger than 5 mm, peripheral nerve autograft remains the gold standard of treatment.[2,4,9] However, the list of risks and potential complications remains numerous, with only 25% of patients achieving a significant level of functional recovery.[10] Risks of autologous grafts include the need for a second surgery to harvest the donor tissue, limited tissue availability, mismatching nerve size/structure, donor site morbidity, and painful neuroma formation.[4,9,11]

New repair strategies developed through nerve tissue engineering and regenerative medicine have focused on developing nerve guidance conduits (NGC) to guide nerve regeneration, and provide an environment supportive of axonal growth and functional neural recovery without painful neuroma formation.[8] There are several NGCs that have been approved by the US Food and Drug Administration (FDA).[2,12] These NGCs are composed of different materials, with various sizes and degradation times, that lessen complications such as those that come with the need for a second surgery, and minimizing the risk of painful neuroma formation.[12] However, available NGCs cannot ensure neural regeneration and functional recovery. As such, ongoing research continues to investigate different materials, biotechnologies, and engineering strategies to improve upon these limitations.[12]

For this study we have developed an NGC composed of poly (lactic-co-glycolic acid) (PLGA) and graphene oxide (GO) that can be seeded with mesenchymal stem cells (MSCs) and with the overall goal of developing a more effective treatment for PNI. PLGA, an FDA-approved type of synthetic polymer, was selected as the base for the scaffold due to its biocompatibility and tunable mechanical and degradation properties, which have been shown to be favorable for neural applications.[13–15] PLGA also has ease of processability and printability allowing precise 3D printed replicates to be made.[13,16] We selected GO, the oxidized form of graphene, to be incorporated into the PLGA because of GO's numerous hydroxyl groups and rough surface area that have

been shown to improve the physicochemical properties, surface topography, and electrical conductivity properties of the scaffold, all of which may beneficially influence cell behavior in favor of functional nerve repair.[16–20] Finally, MSCs were added to the construct because of their potential to self-renew, proliferate, and differentiate into neural and glial lineage.[21–23] MSCs also provide immunomodulatory and neuroprotective effects that allow for restorative neurogenesis, angiogenesis, and synapse formation.[22–25] These cells have been shown to alter the environment post-injury by reducing glial scar formation, reactive oxygen species (ROS) production, and apoptotic behavior, promoting more favorable outcomes.[22,23,26]

We hypothesized that a PLGA conduit, functionalized with GO, would support peripheral nerve regeneration similar to that of an autograft and that addition of MSCs would improve and enhance tissue healing. This study aimed to develop a 3D printing method for PLGA and PLGA/GO NGCs: to assess the effect of these NGCs, with and without MSCs, on peripheral nerve repair; and compare these with that of an autograft over a period of 6-months using a rat sciatic nerve defect model.

Materials and Methods

Materials

All biochemicals, chemicals, and disposable supplies were purchased from Thermo Fisher Scientific (Waltham, MA, USA) unless otherwise noted.

Preparation of Mesenchymal Stem Cells

MSCs were obtained from adipose tissues removed from human patients undergoing panniculectomy at the University of Tennessee Medical Center. Patient consent was obtained as approved by an IRB protocol (IRB protocol #3995). Human adipose tissue derived MSCs were isolated, characterized, and expanded as described previously. Cell adhesion, morphology, protein markers, and trilineage differentiation were confirmed as described previously.[27–30] Cells from passages 2–5 were used. One million MSCs were seeded on the scaffolds for the PLGA/GO+MSC treatment group.

Cytocompatibility of Graphene Oxide

Preparation of PLGA and PLGA/GO coverslips: weight proportions of 0, 0.25, 0.5, and 1% single layer graphene oxide (Cheap Tubes Inc., Grafton, VT, USA) were added to poly (D, L-lactic-co-glycolide) (75:25 lactide: glycolide; MW 30,000–60,000) (Sigma-Aldrich, St. Louis, MO, USA) to synthesize 1 g samples. The PLGA without GO was used as the experimental control. The samples were placed in an Isotemp™ hybridization incubator at 85°C, mixing occasionally, until fully homogenized. A thin layer of PLGA or PLGA/GO material was coated on the glass coverslips. Coverslips were placed into 24-well plates and sterilized under UV light for 4 hours. Ten thousand MSCs were manually seeded on each PLGA and PLGA/GO coverslip. The cell-loaded scaffolds were incubated at 37 °C and 5% carbon dioxide (CO_2), in Dulbecco's modified eagle medium (DMEM) with 10% fetal bovine serum (FBS), and 1% penicillin/streptomycin, for 7 days.[31] Cells were stained with 5mM Calcein AM solution to test for cytocompatibility and cell attachment as previously described.[27,28,32] For staining, cells were incubated at 37 °C for 5 minutes. Fluorescent images at 488 nm and 10X magnification were taken immediately after incubation, using a Leica DMi8 microscope (Leica Microsystems Inc., Deerfield, IL, USA.).[31] Fiji/Image J software was used to obtain data for cell spreading area (μm^2), measured using the freehand selection tool drawn around the periphery of the cell. "Measure" was selected, and area documented.[17,32] Microsoft excel was used to calculate the mean and standard deviation values. GraphPad was used to perform *t*-tests for statistical significance ($p \leq 0.05$).

Synthesis of the Nerve Guidance Conduits

Preparation of PLGA and PLGA/GO conduits: two thousand milligrams of poly (D, L-lactic-co-glycolide) (50:50 lactide: glycolide; MW 30,000–60,000) (Sigma-Aldrich, St. Louis, MO, USA) was blended together with 0.5 mL dimethyl sulfoxide (DMSO) hybri-max™ (MW 78.13 g/mol) (Sigma-Aldrich, St. Louis, MO, USA) in a scintillation vial. For NGCs containing GO, 5 mg single layer graphene oxide (Cheap Tubes Inc., Grafton, VT, USA) was added to the PLGA polymer blend. The blend was placed in an Isotemp™ hybridization incubator at 85°C, for 2.5 hours, at a medium/low

rotisserie speed, mixing occasionally. The vial was placed in a −20°C freezer overnight. The material was placed into the syringe of the thermoplastic printhead of an extrusion-based 3D bioprinter (Cellink Bio X6™, BICO, Göteborg, Sweden). The dimensions were set to 2.75 mm x 2.75 mm x 15 mm (X x Y x Z) and a 0.2 μm printhead nozzle size was used. The printing parameters were set to 200 kPa pressure, 1 mm/sec speed, and 85°C temperature, and adjusted slightly as needed to produce the NGC. NGCs were stored at −20°C long-term, and sterilized under UV light for 2 hours.

Degradation Properties

A PLGA/GO NGC was placed under specific conditions, simulating storage shelf life, to determine post-manufacturing changes in material characteristics. Changes in material characteristics were determined by changes in weight, length, and outer diameter. A PLGA/GO scaffold was left in a 60mm dish at room temperature for 56 days. Daily, the scaffold was weighed using an analytical balance, and the length and outer diameter were measured using a digital caliper. Additionally, two PLGA/GO scaffolds were placed in a dynamic degradation reactor, suspended in 1X PBS, with a continuous peristaltic pump, at 37°C and 5% CO_2 for 21 days. Weekly, the scaffolds were removed from the reactor, hung to dry, weighed using an analytical balance, and the length and outer diameter were measured using a digital caliper.[33,34] The datasets were entered into Microsoft excel and the "TREND" Formula was used to extrapolate the time of degradation for the NGCs in the bioreactor.

Characterization of Conduit Surface

One PLGA and one PLGA/GO scaffold were each used for SEM analysis. The NGCs were gold sputter coated for approximately 20 seconds using an SPI Sputter Coater (SPI Supplies, West Chester, PA, USA).[35] Scaffolds were mounted on individual specimen stubs using carbon tape, and imaged using a Zeiss Auriga Crossbeam Focused Ion Beam (FIB)/ Scanning electron microscopy (SEM) instrument with an accelerating voltage of 5kV and 100X magnification (ZEISS, Oberkochen, Germany).

Additionally, one PLGA and one PLGA/GO scaffold were UV sterilized for 2-hours, and each scaffold was placed in a culture test tube. Three million MSCs were stained with DiI solution as previously described.[27] One million DiI stained MSCs were manually seeded on each: the PLGA scaffold, PLGA/GO scaffold, and a positive control culture dish. The cell-loaded scaffolds were incubated at 37 °C and 5% CO_2, in DMEM with 10% FBS, and 1% penicillin/streptomycin, for 24 hours. The cell-loaded scaffolds were fixed with 4% paraformaldehyde (PFA) at room temperature for 10 minutes, and rinsed twice with Hanks' balanced salt solution (HBSS). The fixed scaffolds were stored at 4 °C for 24 hours. The scaffolds were imaged using a Leica SP8 white light laser confocal microscope (Leica Microsystems Inc., Deerfield, IL, USA).

Animals

Lewis rats (Charles River Laboratories, n=27, male, aged 2 to 3 months) were acclimated prior to beginning procedures. All procedures were conducted in accordance with PHS guidelines for the humane treatment of animals under approved protocols established through the University of Tennessee's Institutional Animal Care and Use Committee (IACUC; protocol # 2574-0921).

Sciatic Nerve Defect Rat Model

Rats were divided into four treatment groups: 1) autograft (positive control; n=8), 2) PLGA NGC (n=6), 3) PLGA/GO NGC (n=6), and 4) PLGA/GO+MSC NGC (n=6). Sciatic nerve defects were individually performed on a total of 26 rats. Rats were weighed (range 250 to 350g) prior to being anesthetized using inhalant isoflurane. The right leg was shaved and prepared for surgery with isopropyl alcohol and chlorhexidine. Buprenorphine (0.05 mg/kg) was administered subcutaneously prior to surgery. The sciatic nerve defect peripheral nerve injury model was created by cutting a 10-mm mid-thigh section of the sciatic nerve.[36–40] Using a microscope guided dissection, an approximately 2-cm linear incision was made through the skin and muscle bellies of the thigh to reach the level of the sciatic nerve. A ruler was used to mark a 10-mm segment, which was sharply excised and removed. The removed sciatic nerve segment was sutured back into its normal anatomical alignment for those in the autograft group. In the remaining three groups, the NGC was positioned in place, spanning the defect gap, and sutured to the transected proximal and distal ends. The

muscles and skin of the surgical site were sutured, and tissue glue was applied over the incision. An E-collar was placed on each rat for 24 hours after surgery. Rats were individually housed and monitored twice daily for the first 3-days, daily for 1-week, and weekly until the end of the 6-month study. Buprenorphine was administered every 12-hours for 3-days after surgery. Baytril (100 mg/400 mL) mixed into water with flavored Gatorade, was provided for 1-week after surgery. One rat was removed at the 5-month timepoint due to excessive environmental stress, unrelated to the project.

Evaluation of Biomechanics and Gait Analysis

Gait patterns were recorded and analyzed at baseline, 2 weeks, and monthly through the 6-month study, using a pressure sensor mat (Tekscan, Inc., Boston, MA, USA) as previously described.[41,42] The associated WALKWAY™ 7.7X computer software was used to assess the stance time (seconds), stride length (cm), and maximum force (kg, controlled for body weight %BW) between the left (untreated) and right (treated) hindlimbs.[40–42] Data sheets were exported to Microsoft excel, and mean and standard deviation values were obtained. GraphPad was used to perform t-tests for statistical significance ($p \leq 0.05$).

Histological Examination of Nanoparticle Translocation

After rat sacrifice at the 6-month timepoint, the lungs, kidneys, liver, and spleen were removed from 3 randomly selected rats from each of the PLGA, PLGA/GO, and PLGA/GO+MSC treatments groups. Tissues were placed in 3% glutaraldehyde for 24 hours. The collected tissues were roughly cut, using a razor blade, into a smaller sample for each tissue, for each rat. The samples were processed using a 4-step ethanol dehydration, ending in 100% ethanol solution. The samples were further processed using a 4-step resin embedding, ending in 100% resin. The samples were polymerized in a 60 °C oven for at least 48 hours. The tissues were roughly isolated using a razor blade, before using a microtome fitted with a glass knife to reveal an even sample section. Using a Leica EM UC7 Ultramicrotome (Leica Microsystems Inc., Deerfield, IL, USA) fitted with a diamond knife, the samples were sectioned 100 µm thick onto gilder grids (Electron Microscopy Sciences, Hatfield, PA, USA). Each grid sample was stained with uranyl acetate and lead citrate. The grids were assessed using transmission electron microscopy (TEM) (JEOL JEM 1400-Flash), to identify the presence of graphene nanoparticles.[43–45] Five to ten images were taken per grid.

Immunohistochemistry Staining and Analysis

At the 6-month end-of-study timepoint, the sciatic nerve was identified and excised a few millimeters beyond the proximal and distal ends of the defect site. Each tissue was aligned on cardboard and placed in a tissue embedding cassette in 10% formalin. Tissues were paraffin embedded and longitudinally sectioned. Each tissue section was deparaffinized in Xylene for five minutes, three times. The sections were placed in 100% ethanol for ten minutes, two times, and 95% ethanol for ten minutes, two times. The sections were washed in deionized water (dH_2O) prior to placing in the 1X citrate unmasking solution (Cell Signaling Technology, Inc., Danvers, MA, USA) at 95–98 °C for 10 minutes, using a microwave oven. The sections were cooled for 30 minutes and washed in dH_2O. The sections were placed in hydrogen peroxide (H_2O_2) for 10 minutes, and washed in dH_2O. The sections were placed in 1X Tris-buffered saline with 0.1% Tween 20 (TBST) for five minutes prior to adding the blocking solution, TBST with 5% goat serum (Cell Signaling Technology, Inc., Danvers, MA, USA) for 1 hour. The primary antibody was added to the sections and left overnight in a humidified chamber at 4 °C. One histology section from all specimens were stained with hematoxylin and eosin (H&E) (Azer Scientific, Inc., Morgantown, PA, USA) for assessment of cellular detail. Immunohistochemistry was performed using myelin basic protein (MBP) (1:500; Cell Signaling Technology, Inc., Danvers, MA, USA), and class III beta tubulin (TuJ1) (1:500; Biolegend, San Diego, CA, USA). MBP was used as a marker of myelin and is associated with myelin sheaths; TuJ1 was used as a marker for neurons, specifically axonal growth by elongation. Sections were washed in TBST prior to adding the secondary antibody to the sections in the humidified chamber for 1 hour at room temperature. The secondary antibodies used were: goat anti-rabbit IgG HRP (Boost IHC Detection Reagent, Cell Signaling Technology Inc., Danvers, MA, USA), and rabbit anti-mouse IgG HRP (Abcam, Cambridge, UK). Sections were washed in TBST prior to adding the DAB solution (30 µL chromogen concentrate in 1 mL diluent) (Cell Signaling Technology, Inc., Danvers, MA, USA) for 10 minutes. Sections were washed in dH_2O prior to dehydrating the samples

my immersing briefly in 95% ethanol, two times, 100% ethanol, two times, and xylene, two times. Sections were mounted using mounting medium (Cell Signaling Technology, Inc., Danvers, MA, USA) and a cover slip. The H&E sections were analyzed by a trained histologist for local adverse effects. The MBP and TuJ1 sections were imaged using Keyence BZ-X Series All-In-One Fluorescent Microscope (Keyence Corporation of America, Itasca, IL, USA) at 20X magnification. For each section, multiple images were taken along the length of the section with 20% overlap and stitched together to create a single image of the entire section. Scale bars were added. ImageJ software was used to analyze the stitched images.[40] They were selected for optimal contrast (blue) and threshold (155–255). The nerve was isolated from the background and converted to a black and white image (black = stained tissue). For each section the nerve was measured for total area (mm^2), and percent area (percentage of black in the image; %). Microsoft excel was used to multiply the total area by the percent area, to obtain the stained area (mm^2). Mean and standard deviation values were obtained. GraphPad was used to perform t-tests for statistical significance ($p \leq 0.05$).

Gross Muscle Weight and Length Analyses

After rat sacrifice, the left and right hind limbs from each rat were removed at the hip joint and placed in formalin for 48-hours, with the ankle and knee joints pinned at 90° angles. The hindlimbs were then placed in 70% ethanol until muscle dissections were complete. The skin was removed, and the fascia was cut to separate the muscles. The soleus (S), medial gastrocnemius (MG), and lateral gastrocnemius (LG) muscles were identified, isolated, and removed at the sites of origin and insertion: these muscles were chosen because they are innervated by the tibial nerve, a branch of the sciatic nerve, and are major contributors to ankle function during walking gait.[46,47] Any remaining tendon, after muscle removal, was removed. Each muscle was weighed with an analytical balance, and measured for length three times with a digital caliper.[48–51] Microsoft excel was used to document the datapoints and obtain the mean and standard deviation values. GraphPad was used to perform t-tests for statistical significance ($p \leq 0.05$).

Results and Discussion

In vitro Material Characterization

The rough surface area, numerous hydroxyl groups, and conductive properties that GO provides are known to beneficially influence cell behavior in favor of functional nerve regeneration.[17–20] Despite these desirable physicochemical properties, GO has much controversy over its cytotoxicity and use in vivo. Some reviews cite toxicity as low as 0.01%, while others report no signs of toxicity as high as 6%.[52] GO has the potential to negatively affect cells by internalizing nanoparticles through phagocytosis or membrane damage. This increases ROS and inflammation that cause mitochondrial dysfunction, leading to cell death.[19,53–56] Contrarily, GO may beneficially disturb dysregulated mitochondrial pathways, or initiate an adaptive process of cellular protection when trauma exists.[55,56] Variables such as surface functionalization, particle shape and size, dispersion, concentration, dosage, route of administration, and processing techniques can all influence whether GO exhibits toxic behavior.[19,52–54,57–59] Therefore, we evaluated, in vitro, GO in three concentrations while maintaining the same synthesis and processing variables as our NGC. By day 7 in vitro, MSCs attached to the PLGA/GO coverslips for all iterations of GO concentration (Figure 1A–D). Overall, the Calcein AM staining showed strong expression of the green fluorescence across the different GO concentrations. This indicates a good cell viability on the PLGA/GO material. However, there was a clear difference in cell attachment and morphology on the 0.25% GO and 0.5% GO. There appeared to be more cells attached across these materials, and the cells were spread over larger areas. Increased cell spreading has been known to indicate improved cell attachment and cell-to-cell communication for a more cohesive tissue architecture.[31,60,61] When the cell spreading area was quantified, the results confirmed our observations, showing a significantly increased cell spreading area on the 0.25% GO and 0.5% GO concentrations as compared to the PLGA and 1% GO materials (Figure 1E). With this knowledge, our study pursued the fabrication of a PLGA/GO NGC using a 0.25% wt. concentration. Choosing a lower concentration allowed us to begin at a starting point that can be increased in future studies.

The weight, length, and outer diameter were evaluated to understand how the NGC degrades after printing, and through implantation. At room temperature, there were no changes in material size and weight for 56 days (Figure 2A and B). The material was shown to be stable under standard room conditions, allowing for simple storage prior to implantation. However, further study

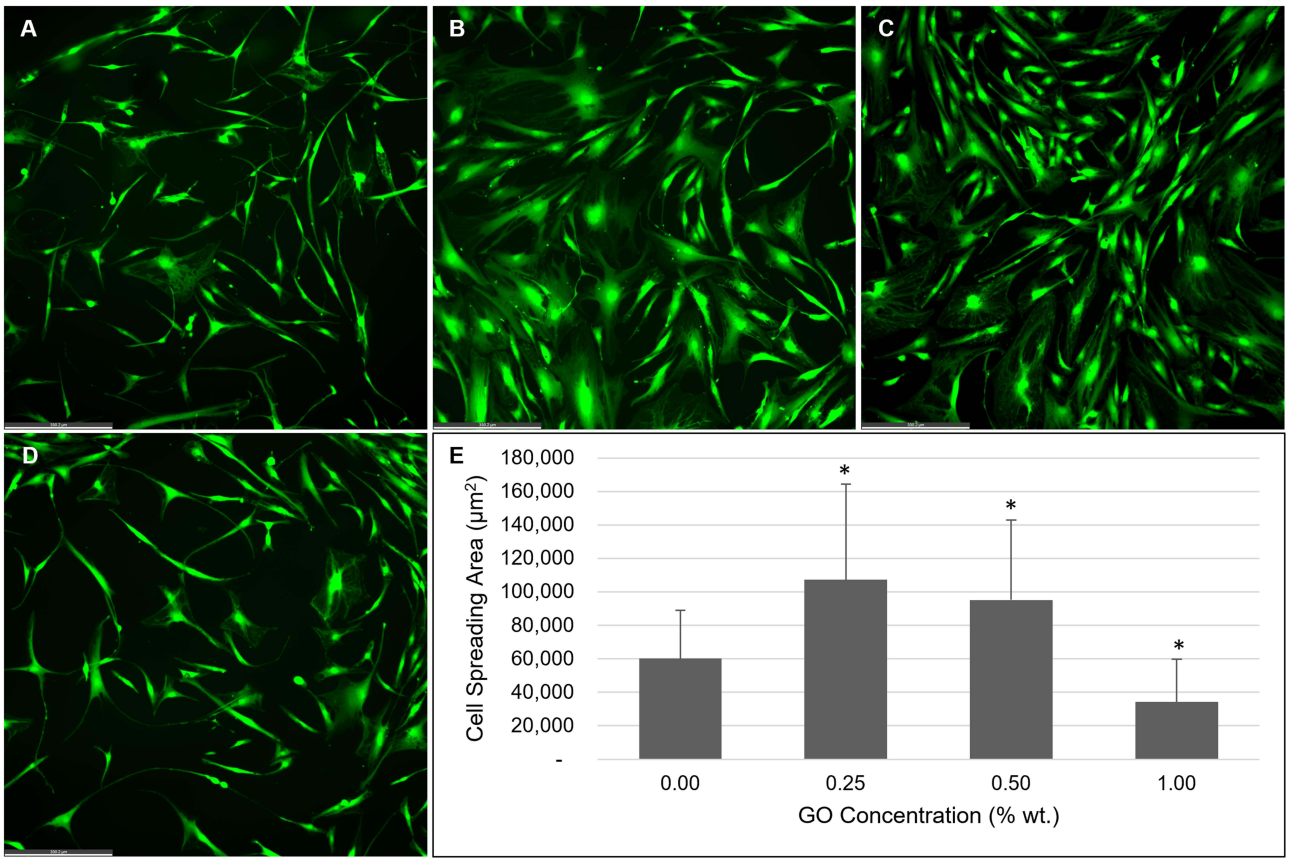

Figure 1 Representative fluorescent images (10X) of (**A**) PLGA, (**B**) 0.25% GO, (**C**) 0.5% GO, and (**D**) 1% GO visualize MSC attachment, cell spreading, and cell viability. (**E**) Graph quantitates cell spreading area of each iteration of GO concentration. PLGA/GO coverslips with 0.25% GO and 0.5% GO exhibited the greatest cell spreading area. *p ≤ 0.05.

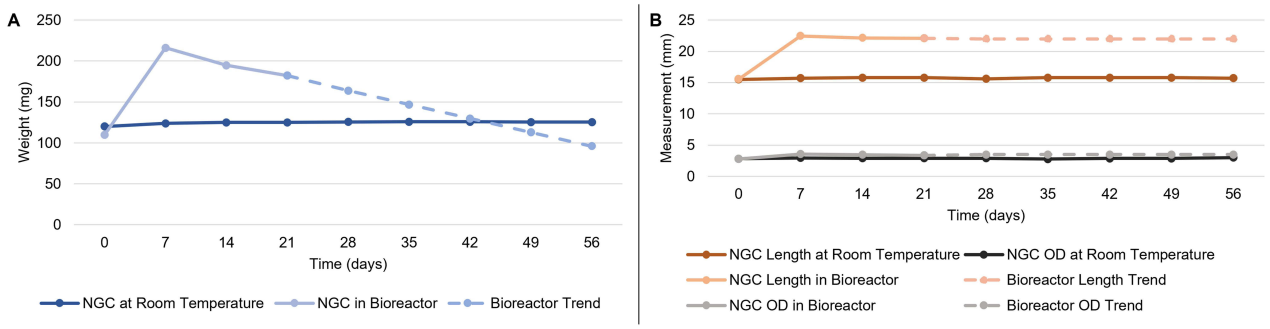

Figure 2 Determining in vitro degradation of the PLGA/GO NGC. (**A**) At room temperature the NGC maintains weight through day-56, and in a bioreactor the weight increases the first week, then decreases through day-21. (**B**) At room temperature the NGC maintains length and outer diameter measurements through day-56, and in a bioreactor the length increases the first week, then maintains through day-21, while outer diameter maintains throughout the study.

is needed to determine the maximum shelf-life of the material. The PLGA/GO NGCs placed in a bioreactor for 21 days exhibited no changes in outer diameter. However, there was a 44.4% increase from the original length in the first week that was then maintained through day 21 (Figure 2B). The weight also had a 96.7% increase from the original weight in the first week, followed by a slow decrease through day 21 (Figure 2A). The initial weight increase was expected and is most likely due to PLGA's hydrophilic nature to absorb water.[33,62] The degradation in mimicked physiological conditions showed a slow degradation over the 21 days. If the degradation rate were to continue to trend steadily in this direction, the material would be expected to fully degrade in approximately 3–4 months. This is consistent with previous studies of PLGA degradation.[63]

https://doi.org/10.2147/IJN.S501241

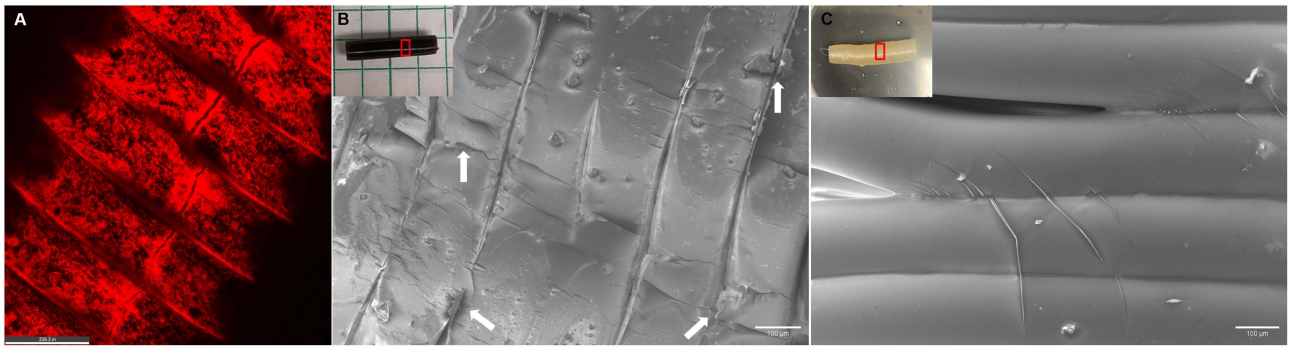

Figure 3 Confocal image (10X) of (**A**) the exterior side of the PLGA/GO NGC shows DiI-labelled MSCs confirming cell attachment after 24-hours in vitro, and are representative of similar internal surfaces. SEM images of the outer surface of the (**B**) PLGA/GO and (**C**) PLGA NGCs and are representative of similar internal surfaces. Arrows indicate rougher areas on the PLGA/GO surface.

Additionally, DiI-labelled MSCs incubated on the PLGA/GO NGC for 24 hours attached across the surface both within and on the outside of the conduit (Figure 3A). Attachment was greater on the PLGA/GO NGC as compared to the PLGA NGC, which showed little cell attachment (data not shown). This confirms that the MSCs attached to the PLGA/GO NGC prior to implantation for the in vivo study, and the addition of GO improves cell attachment.[57,64] This improved cell attachment may be due to the increased surface roughness driven by the addition of GO. SEM images of the PLGA and PLGA/GO NGCs visualize the differences in surface topography between the two conduits (Figure 3B and C). Subjectively, we observed a rougher surface when GO was added to PLGA. The rougher surface is expected to have an increased surface area, which is known to promote increased cell attachment for improved cell behavior.[57,64,65]

In vivo Implantation of Conduit Into Sciatic Nerve Defect Rat Model

Although other treatment options, such as allografts, exist, the current "gold standard" of treatment is surgical intervention using an autograft. Implanting an autograft requires two surgeries, one to harvest the healthy nerve, and another to implant at the site of injury. This comes with numerous risks including those associated with two surgeries, donor site morbidity due to neuroma formation and associated pain, and issues with dimensional mismatch in terms of nerve size and axon alignment.[12] However, autografts often result in poor functional outcomes with limited functional recovery.[8] The autologous group served as the positive control for comparisons with the experimental NGC groups. Additionally, the 15mm NGC fitted into the 10mm defect with

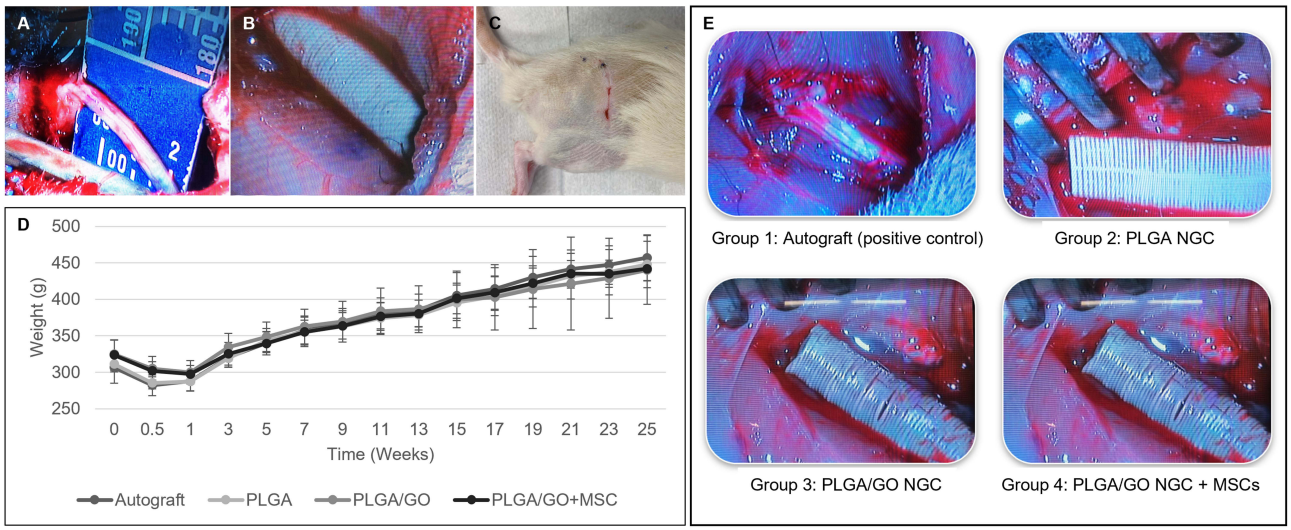

Figure 4 Surgical implantation of four treatment groups and post-surgical recovery. (**A**) The creation of the 10-mm sciatic nerve defect. (**B**) The sutured NGC into the defect site. (**C**) The healing surgical site 1-week post-surgery. (**D**) Rat weights showed an initial decrease at 1-week post-surgery followed by a steady increase over the 6-month study period, with no differences between each treatment group. (**E**) Each rat received one of four treatment groups: autograft (positive control), PLGA NGC, PLGA/GO NGC, and PLGA/GO+MSC NGC.

sufficient excess length on either side to allow suturing of the material to the severed proximal and distal neurolemma (Figure 4A and B). The PLGA/GO material was easy to handle and suture, maintaining shape and structure throughout the implantation surgery, to prevent kinks and provide continuity to the growing axons during the healing process. Surgeon feedback confirmed that these features of the NGC improved the efficiency of the graft procedure as compared with that of the autograft. After surgery the rats were monitored and weighed regularly (Figure 4C and D). The incision site healed normally for all rats, with no signs of rejection, or localized adverse events. There was an initial drop in rat weight 1-week after surgery which was expected as the rats recovered and were less active. After 1-week, the rats steadily increased in weight over the 6-month time period. All rats showed no signs of pain, based on the rat grimace scale's evaluation of orbital tightening, nose flattening, and ear and whisker changes. Observationally during each weight assessment, all rats exhibited normal behavior, including grooming and interaction with enrichment toys.[66] There were no differences in weight or behavior at any timepoint across the four treatment groups. Each rat having received a sciatic nerve defect was treated with one of these four treatment groups: an autograft, a PLGA NGC, or a PLGA/GO NGC with or without MSCs (Figure 4E). Each group was selected to isolate a variable and ensure any differences seen as compared to the autograft can be explained by either the PLGA, GO, or MSC component. At the end of the 6-months, the PLGA scaffolds were fully degraded. The nerves harvested from the PLGA/GO and PLGA/GO+MSC groups showed graphene incorporated in the local tissue, but there was no PLGA or NGC structure remaining.

Graphene Accelerated the Return to Presurgical Levels of Maximum Vertical Ground Contact Force

An analysis of pressure mat kinematics revealed no significant differences in stance time and stride length between the four experimental groups at any of the evaluated timepoints. However, there were also no changes in these parameters over time, which was unexpected.[41] There were significant differences in the maximum vertical ground contact force between the left and right hindlimbs, when controlled for body weight. Each rat was evaluated pre-surgery to establish a baseline, after multiple practices in the weeks leading to the official baseline reading. Each rat was also evaluated at 2 weeks, 2 months, 5 months, and at the end of the study period 6 months after surgery. All the groups (autograft, PLGA, PLGA/GO, and PLGA/GO+MSC) showed significant increases in their maximum force ratios (p-values: 0.0005, 0.006, 0.01, and 0.02 respectively) at 2-weeks after surgery as compared with the baseline (Figure 5). This showed that all rats were transferring weight to their left hindlimb (untreated) and

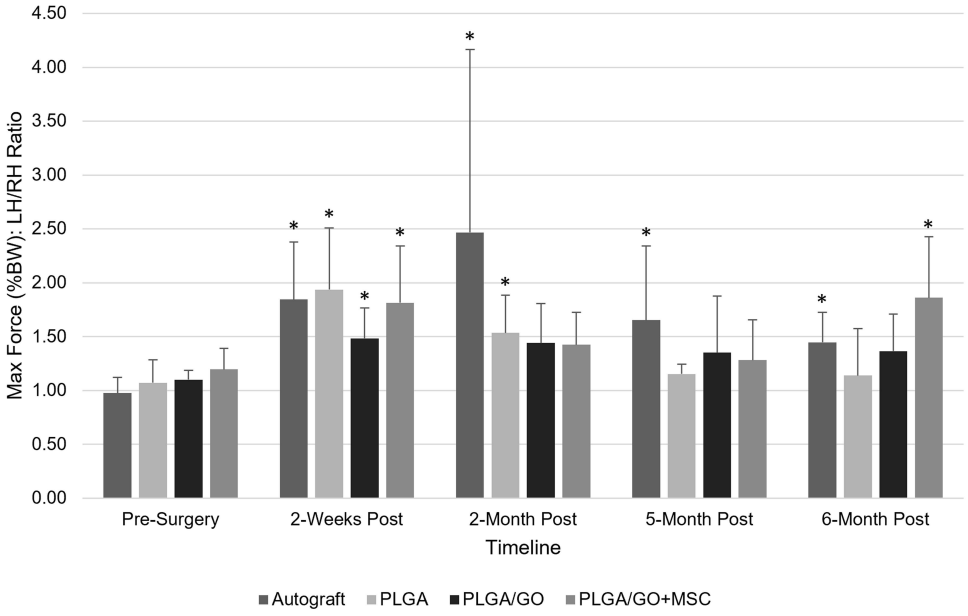

Figure 5 Pressure mat evaluation over 6-month time period for autograft, PLGA, PLGA/GO, and PLGA/GO+MSC groups. Pressure mat evaluation measured maximum force as a ratio of left hindlimb over right hindlimb, adjusted for percent body weight. As compared to pre-surgery levels, all groups showed a significant increase in max force at 2-weeks post-surgery. PLGA showed no significant differences at 5, and 6-months post-surgery. PLGA/GO showed no significant differences at 2, 5, and 6-months post-surgery. PLGA/GO+MSC showed no significant differences at 2, and 5-months post-surgery. *p ≤ 0.05.

https://doi.org/10.2147/IJN.S501241

off-loading use of their right hindlimbs (treated) at this time point. This is expected with this model of severe PNI. Over the 6-month duration of study, the autograft group did not return to pre-surgical force values, remaining significantly different at the 2-month, 5-month, and 6-month timepoints (p-values: 0.03, 0.02, and 0.0009 respectively). Surprisingly, the PLGA group returned to pre-surgical use of both hindlimbs at the 5-month and 6-month timepoints, showing no significant differences to the pre-surgery levels. Qualitatively, during pressure mat evaluations, the PLGA group did not move their hindlimbs as much as the other groups, but the rats accommodated by placing their weight on the treated leg to walk. We hypothesize that the rats in this group had no sensory or motor functions in their treated limbs. The PLGA/GO group returned to pre-surgery hindlimb use by the 2-month timepoint, showing no significant differences at the 2-month, 5-month, and 6-month timepoints as compared to the pre-surgery levels. Qualitatively, these rats exhibited a normal range of motion of their hind legs while walking on the pressure mat. The PLGA/GO+MSC group also returned to pre-surgery hindlimb use in the 2-month and 5-month timepoints, showing no significant differences as compared to the pre-surgery levels. Interestingly, at the 6-month timepoint, these rats were significantly different than the pre-surgical level (p-value 0.02). We hypothesize that this shift may be due to either the addition of MSCs causing an inhibition in the conduit's repair long term, or a need for additional MSCs over longer healing periods. Further investigation is needed to understand why this occurred.

No Evidence of Nanoparticle Translocation Was Identified

Despite the many desirable physicochemical properties of GO, there remains controversy over potential cytotoxicity when used in vivo. This is primarily due to the numerous variables that can impact the biocompatibility of graphene.[52–54,59] While it remains unknown how graphene is excreted from the body, some studies have reported evidence of nanoparticles in the cytoplasm of human cell lines, locally at the site of administration, and in organs, including liver, lung, spleen, kidney, brain, heart, small intestine, and reproductive organs. Autophagy of GO can cause cell apoptosis, resulting in an inflammatory response that further damages the local area, while the aggregation of nanoparticles in our body's filtering systems can prevent these organs from functioning properly and lead to systemic issues.[52,56,59,67] For this study, we chose the kidney, lung, spleen, and liver to identify if the graphene nanoparticles, implanted in the PLGA/GO NGC, could be identified in these tissues as a part of the body's attempt to filter out foreign material.[67,68] Multiple tissue sections and grids were reviewed from rats that either had GO as part of the implanted NGC or that had no GO implanted. Normal tissue structures were seen for kidney, and lung sections.[44] Liver and spleen sections were unable to be obtained and imaged due to challenges in tissue processing and sectioning. No evidence of graphene nanoparticles was seen in the cells and surrounding structures of the kidney or lung tissues observed, as compared to previous descriptions (Figure 6A–D).[43,67,69] This may be due to how the GO flakes were processed and incorporated into our NGC, the low percentage that was used (0.25%), or the possibility that the implantation at the site of injury held the nanoparticles in the recovering area instead of attempting to remove them through these systems. These results may indicate that our PLGA/GO NGC may be safely implanted without nanoparticles being translocated to the kidney and lung, causing injury in sites remote from the site of implantation. Further investigations will be needed into additional routes, such as the liver, spleen, and lymph nodes. Future studies may also evaluate the long term implications of graphene nanoparticles remaining at the site of implantation.

Immunohistochemistry of Sciatic Nerve Tissue

Tissue sections were stained with MBP and TuJ1 antibodies to identify differences in myelin and neural tissue growth respectively, between the different treatment groups. Qualitatively, the tissue organization of the PLGA group looked abnormal, while the PLGA/GO, PLGA/GO+MSC, and autograft groups looked comparable to the normal nerve tissue, collected from the contralateral hindlimbs of the treated rats. The PLGA/GO and PLGA/GO+MSC groups had GO remaining in the area of the defect, with incorporation into the repaired neural tissue (Figure 7A). Additionally, the overall tissue structure of the three experimental groups was more similar to the normal nerve with an aligned axonal growth, and no evidence of neuroma formation (Figure 7B). This may be due to the shape of the hollow NGC design, which acts as a guide providing cues for the newly developing tissue.[70]

The myelin sheath is composed of proteins and lipids with MBP as one of the primary proteins in this composition, and playing an important role in maintaining myelin structure.[71] When assessing the area (mm^2) stained with MBP, there were no differences in the three experimental groups as compared to the autograft (Figure 7C). However, the PLGA/GO

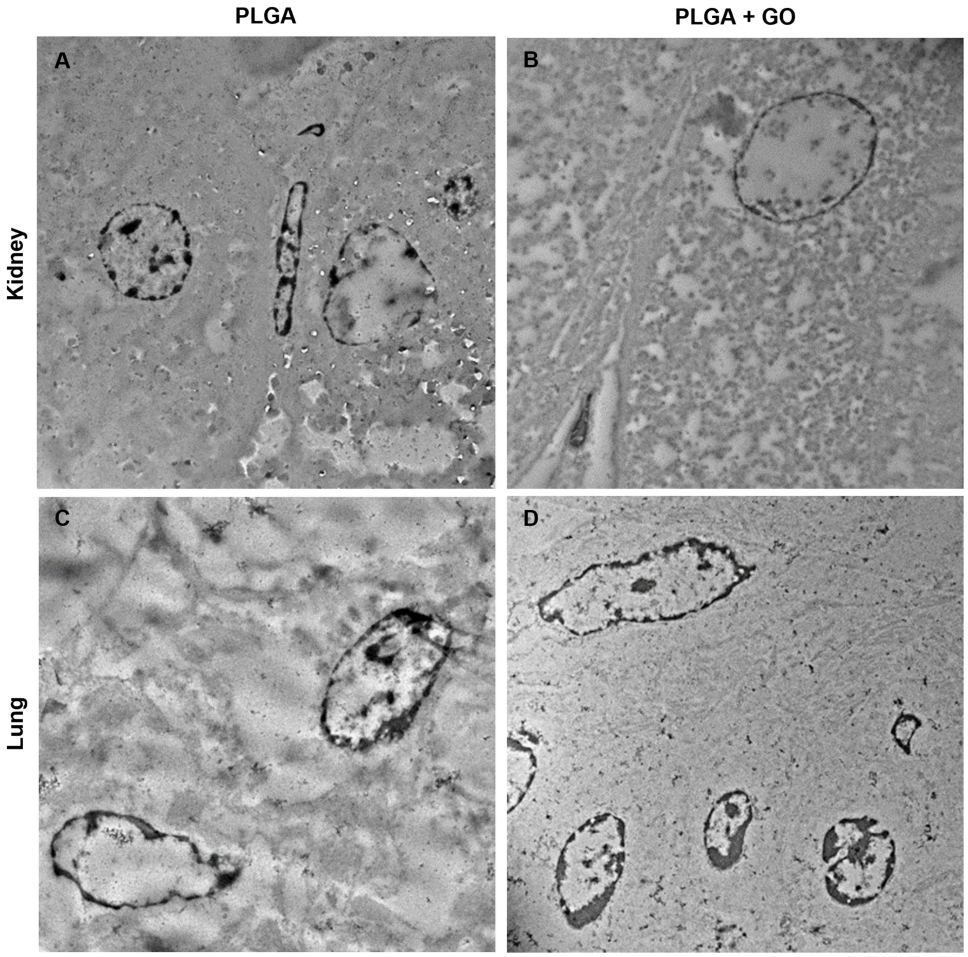

Figure 6 Representative TEM images of kidney tissue isolated from the (**A**) PLGA NGC and (**B**) PLGA/GO NGC treatment groups, and lung tissue isolated from the (**C**) PLGA NGC and (**D**) PLGA/GO NGC treatment groups.

group was significantly greater than the PLGA group (p-value 0.01). Compared to the normal nerve, there were no significant differences with the two groups containing GO, but the normal nerve had significantly greater MBP-stained area than the autograft and PLGA groups (p-values 0.009, and 0.0004 respectively). This may indicate the addition of GO increases the expression of MBP and growth of the myelin sheath to pre-injury levels.

Axonal regeneration in the peripheral nervous system and the rate of axonal growth are key features of the neuronal-specific tubulin isoform, TuJ1.[72] Both the PLGA/GO and PLGA/GO+MSC groups were significantly greater than the PLGA (p-values: 0.005, and 0.02 respectively) and autograft (p-values: 0.03, and 0.02 respectively) groups. While the PLGA and autograft groups were not significantly different than the normal nerve, the PLGA/GO and PLGA/GO+MSC groups were significantly greater than the normal nerve (p-values: 0.004, and 0.004 respectively). The increased area of TuJ1 in the experimental groups containing GO may be due to the increased rate of axonal regeneration occurring in the present tissue. However, it also may be due to an experimental error where the remaining GO in the area accounted for a small percentage of the area stained. Future studies may evaluate additional histological markers for greater evidence of physical axonal repair.

The H&E analysis described no definitive local immune reaction, though the neural tissue mixed with the remaining graphene oxide material may represent a target for a future immune response. This would require further long-term investigation beyond the 6-month period this study provides.

https://doi.org/10.2147/IJN.S501241

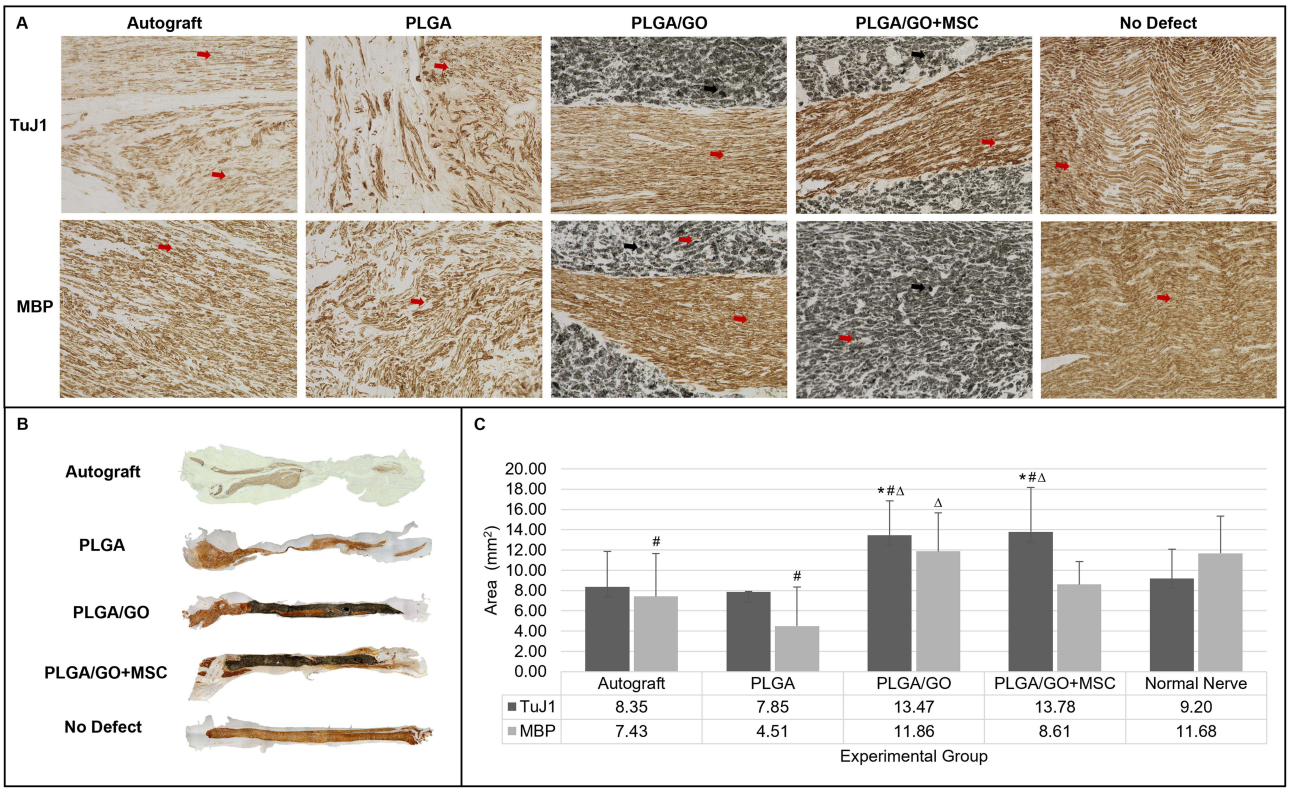

Figure 7 Immunohistochemistry of sciatic nerve showed (**A**) the autograft, PLGA/GO, and PLGA/GO+MSC groups showed tissue organization comparable to the normal nerve (red arrows highlight areas of specific tissue staining and organization, and black arrows indicate areas of incorporated graphene nanoparticles); (**B**) the PLGA, PLGA +GO, and PLGA/GO+MSC groups showed gross structures similar to the normal nerve; and (**C**) the area stained with MBP and TuJ1 in the PLGA/GO and PLGA/GO+MSC groups were comparable to or greater than the normal nerve ($^{*}p \leq 0.05$ as compared to the autograft, $^{\#}p \leq 0.05$ as compared to the normal nerve, $^{\Delta}p \leq 0.05$ as compared to the PLGA group).

Qualitative and Quantitative Differences in Muscle Weight

Gross muscle analysis qualitatively and quantitatively evaluated the muscle length (mm) and weight (g) of the soleus (S), lateral gastrocnemius (LG), and medial gastrocnemius (MG) muscles, forming the hindlimb muscles, downstream of the affected sciatic nerve.[73] Though few "normal" rat muscle lengths have been reported, each muscle was measured with a similar range as previous studies.[74–76] There were no significant differences in muscle length between the four experimental groups for each muscle type, and there were no significant differences in muscle length between the treated and untreated hindlimbs for all muscle groups. Observationally, there were notable differences in the muscle size (Figure 8A). All muscles of the PLGA group were thin and translucent, potentially indicating signs of atrophy when compared to the other groups. There were no obvious differences noted between the autograft, PLGA/GO, and PLGA/GO+MSC groups, meanwhile the muscles of the untreated hindlimbs were visibly larger, fuller, and denser. Quantitatively, when comparing muscle weights, there were significant decreases in the S, MG, and LG of all treated hindlimbs, as compared to the untreated hindlimb (p-values all ≤0.0015) (Figure 8B). While these differences may indicate lesser use of the injured hindlimb, these differences may also be a result of the rats shifting their weight during the initial recovery from surgery to compensate for the healing, treated hindlimb. Isolating the treated hindlimb, the PLGA/GO, and PLGA/GO+MSC groups showed no significant differences from the PLGA group, and all three were significantly decreased than the autograft group (p-values all ≤0.03). Despite contradicting qualitative differences in muscle size, noting the PLGA/GO and PLGA/GO+MSC groups were more comparable to the autograft than the PLGA group, the quantitative muscle weight analysis indicates the PLGA/GO and PLGA/GO+MSC groups were significantly different from the autograft group, and significantly similar to the PLGA group. This suggests innervation of the muscle was not fully re-established. This also contradicts the maximum vertical ground contact force data discussed previously. While there is some evidence of partial reinnervation, further studies are needed to confirm the NGC's capabilities for functional repair.

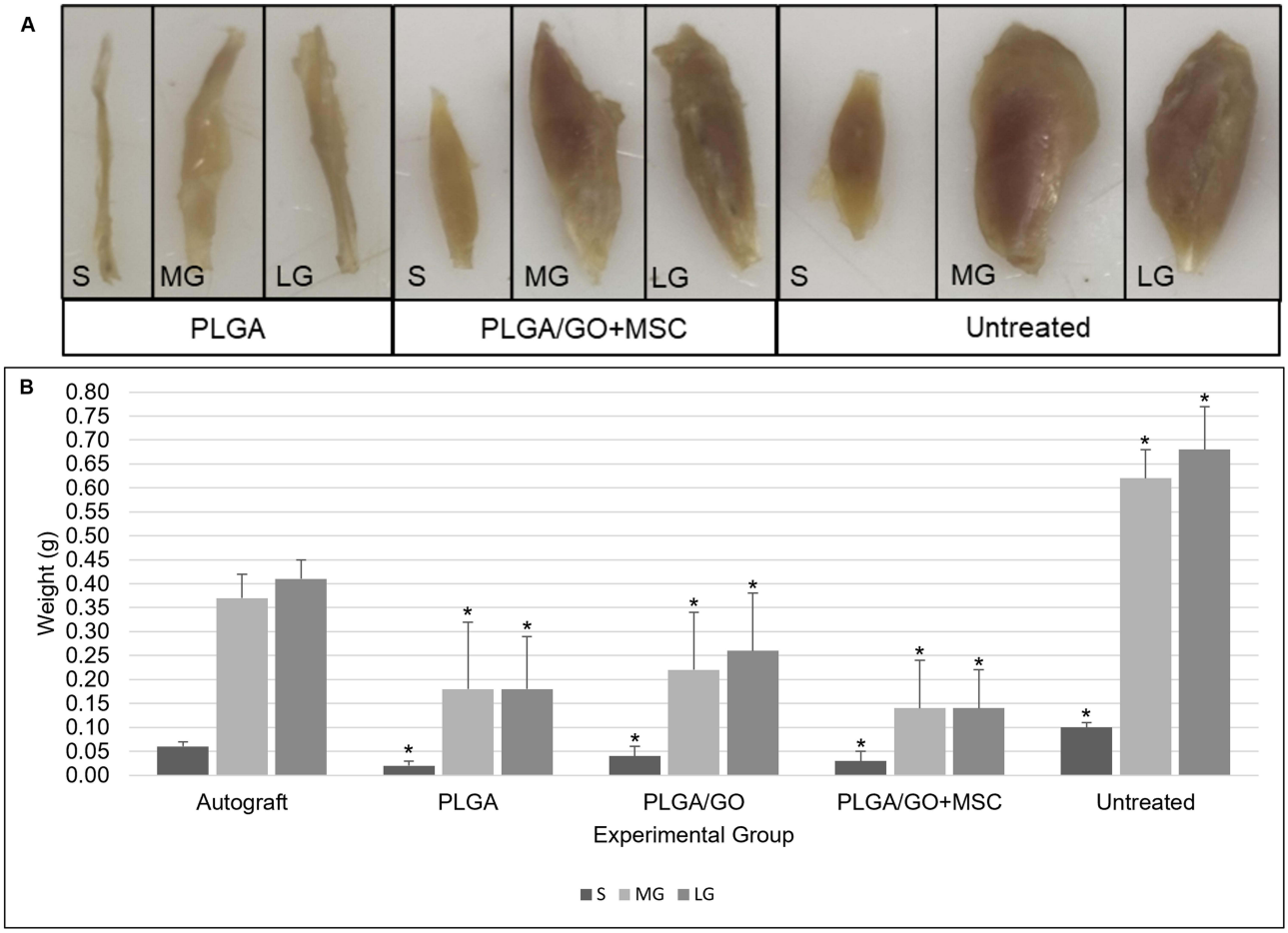

Figure 8 (**A**) Muscle analysis shows qualitatively the PLGA group is decreased in size as compared to the PLGA/GO+MSC group, which is decreased in size as compared to the untreated hindlimbs; (**B**) quantitative evaluation of the muscle weights shows no differences in the PLGA, PLGA/GO, and PLGA/GO+MSC groups, which are all significantly decreased from the autograft group. All treatment groups had significantly decreased muscle weight compared to the untreated group. *$p \leq 0.05$.
Abbreviations: LG, lateral gastrocnemius; MG, medial gastrocnemius; S, soleus.

Conclusions

Using 0.25% GO as a starting point for the PLGA/GO NGC, the construct was successfully synthesized, 3D printed, and evaluated for cytocompatibility in vitro. Future studies may evaluate additional material characteristics of the construct, such as mechanical properties, as well as evaluating the degradative properties with larger sample sizes and for longer periods of time. Further investigation and construct development may also evaluate the use of larger concentrations of GO. The in vivo evaluation determined the NGC to be easy to use surgically, while causing no behavioral changes in the rats, no local adverse effects, and no evidence of translocation of nanoparticles in the kidney and lung tissues. The evidence provided indicates biocompatibility of the construct, though future studies will be needed to further understand the long-term effects of GO nanoparticles remaining in the body chronically. The IHC indicated a physical axonal and myelin repair comparable to or greater than the autograft, as well as a superior neural fiber alignment, possibly due to the guidance provided by the shape of the printed construct. Further studies may expand the IHC staining to advance our understanding of the repaired tissue composition. Finally, the evaluation of the maximum vertical ground contact force showed strong evidence that the addition of GO accelerated the healing for using the injured hindlimb. However, the contradiction of the decreased muscle weights in the experimental groups requires further investigation into the functional repair capabilities of the construct. Future studies may also evaluate the electrophysiological capabilities of the repaired nerve. In all, the addition of MSCs to the PLGA/GO NGC, while remaining biocompatible, did not exhibit any enhanced therapeutic effects in the experiments performed. Future studies may evaluate how to improve the

efficiency of the MSCs, including the use of neural or glial progenitor cells, or 3D cultures. With further investigation, this specific combination of PLGA and GO may provide an effective biomimetic therapy to repair PNIs.

Data Sharing Statement

The datasets generated and/or analyzed during this study are available from the corresponding author upon reasonable request.

Ethics Approval and Informed Consent

The study was conducted according to the guidelines of the Declaration of Helsinki. Human adipose tissue was obtained from patients in accordance with an approved IRB protocol (# 3995) from the University of Tennessee Knoxville. Informed client consent was obtained from the patient prior to the harvest. The animal study protocol was approved by the Institutional Animal Care and Use Committee (IACUC) at the University of Tennessee (IACUC Protocol #2574).

Consent for Publication

All authors consent for publication.

Acknowledgment

The authors acknowledge the assistance of Amber MacDonald in the defect surgery, Jaydeep Kalope for the confocal microscopy and training on the transmission electron microscopy, and Robert Donnell for analysis of the H&E-stained histological slides. Dr. Alisha Pedersen is now affiliated with Powered Research (Research Triangle Park, Durham, NC 27709, USA) following the completion of this research, which was conducted while at the University of Tennessee.

Author Contributions

All authors made a significant contribution to the work reported, whether that is in the conception, study design, execution, acquisition of data, analysis and interpretation, or in all these areas; took part in drafting, revising or critically reviewing the article; gave final approval of the version to be published; have agreed on the journal to which the article has been submitted; and agree to be accountable for all aspects of the work.

Funding

This article was funded by the University of Tennessee: Office of Research, Innovation, and Economic Development Seed Award.

Disclosure

Mrs Meaghan Harley-Troxell reports a patent UTRF 25010-01 pending to UTK. The authors report there are no conflicts of interest in this work.

References

1. (NINDS) NIoNDaS. Peripheral Neuropathy. Available from: https://www.ninds.nih.gov/health-information/disorders/peripheral-neuropathy. Accessed March 11, 2025.
2. Du J, Chen H, Qing L, Yang X, Jia X. Biomimetic neural scaffolds: a crucial step towards optimal peripheral nerve regeneration. *Biomater Sci*. 2018;6(6):1299–1311. doi:10.1039/c8bm00260f
3. Modrak M, Talukder MAH, Gurgenashvili K, Noble M, Elfar JC. Peripheral nerve injury and myelination: potential therapeutic strategies. *J Neurosci Res*. 2020;98(5):780–795. doi:10.1002/jnr.24538
4. Yi S, Xu L, Gu X. Scaffolds for peripheral nerve repair and reconstruction. *Exp Neurol*. 2019;319:112761. doi:10.1016/j.expneurol.2018.05.016
5. Soman SS, Vijayavenkataraman S. Perspectives on 3D bioprinting of peripheral nerve conduits. *Int J Mol Sci*. 2020;21(16). doi:10.3390/ijms21165792
6. Lopes B, Sousa P, Alvites R, et al. Peripheral nerve injury treatments and advances: one health perspective. *Int J Mol Sci*. 2022;23(2). doi:10.3390/ijms23020918
7. Zhang M, Li L, An H, Zhang P, Liu P. Repair of peripheral nerve injury using hydrogels based on self-assembled peptides. *Gels*. 2021;7(4). doi:10.3390/gels7040152

8. Wang ML, Rivlin M, Graham JG, Beredjiklian PK. Peripheral nerve injury, scarring, and recovery. *Connect Tissue Res*. 2019;60(1):3–9. doi:10.1080/03008207.2018.1489381
9. Khaled MM, Ibrahium AM, Abdelgalil AI, El-Saied MA, El-Bably SH. Regenerative strategies in treatment of peripheral nerve injuries in different animal models. *Tissue Eng Regen Med*. 2023;20(6):839–877. doi:10.1007/s13770-023-00559-4
10. de Assis ACC, Reis ALS, Nunes LV, et al. Stem cells and tissue engineering-based therapeutic interventions: promising strategies to improve peripheral nerve regeneration. *Cell Mol Neurobiol*. 2023;43(2):433–454. doi:10.1007/s10571-022-01199-3
11. Zhang F, Zhang M, Liu S, et al. Application of hybrid electrically conductive hydrogels promotes peripheral nerve regeneration. *Gels*. 2022;8(1). doi:10.3390/gels8010041
12. Stocco E, Barbon S, Emmi A, et al. Bridging gaps in peripheral nerves: from current strategies to future perspectives in conduit design. *Int J Mol Sci*. 2023;24(11). doi:10.3390/ijms24119170
13. Guo T, Lim C, Noshin M, Ringel JP, Fisher JP. 3D printing bioactive PLGA Scaffolds using DMSO as a removable solvent. *Bioprinting*. 2018;10: e00038. doi:10.1016/j.bprint.2018.e00038
14. Lu P, Wang G, Qian T, et al. The balanced microenvironment regulated by the degradants of appropriate PLGA scaffolds and chitosan conduit promotes peripheral nerve regeneration. *Mater Today Bio*. 2021;12:100158. doi:10.1016/j.mtbio.2021.100158
15. Dos Santos FP, Peruch T, Katami SJV, et al. Poly (lactide-co-glycolide) (PLGA) scaffold induces short-term nerve regeneration and functional recovery following sciatic nerve transection in rats. *Neuroscience*. 2019;396:94–107. doi:10.1016/j.neuroscience.2018.11.007
16. Harley-Troxell ME, Steiner R, Advincula RC, Anderson DE, Dhar M. Interactions of cells and biomaterials for nerve tissue engineering: polymers and fabrication. *Polymers*. 2023;15(18). doi:10.3390/polym15183685
17. Joseph G, Orme RP, Kyriacou T, Fricker RA, Roach P. Effects of surface chemistry interaction on primary neural stem cell neurosphere responses. *ACS Omega*. 2021;6(30):19901–19910. doi:10.1021/acsomega.1c02796
18. Maleki M, Zarezadeh R, Nouri M, et al. Graphene oxide: a promising material for regenerative medicine and tissue engineering. *Biomol Concepts*. 2020;11(1):182–200. doi:10.1515/bmc-2020-0017
19. Rhazouani A, Gamrani H, El Achaby M, et al. Synthesis and toxicity of graphene oxide nanoparticles: a literature review of in vitro and in vivo studies. *Biomed Res Int*. 2021;2021:5518999. doi:10.1155/2021/5518999
20. Hui Y, Yan Z, Yang H, Xu X, Yuan WE, Qian Y. Graphene family nanomaterials for stem cell neurogenic differentiation and peripheral nerve regeneration. *ACS Appl Bio Mater*. 2022;5(10):4741–4759. doi:10.1021/acsabm.2c00663
21. Priester C, MacDonald A, Dhar M, Bow A. Examining the characteristics and applications of mesenchymal, induced pluripotent, and embryonic stem cells for tissue engineering approaches across the germ layers. *Pharmaceuticals*. 2020;13(11). doi:10.3390/ph13110344
22. Lv B, Zhang X, Yuan J, et al. Biomaterial-supported MSC transplantation enhances cell-cell communication for spinal cord injury. *Stem Cell Res Ther*. 2021;12(1):36. doi:10.1186/s13287-020-02090-y
23. Kaminska A, Radoszkiewicz K, Rybkowska P, Wedzinska A, Sarnowska A. Interaction of Neural Stem Cells (NSCs) and Mesenchymal Stem Cells (MSCs) as a promising approach in brain study and nerve regeneration. *Cells*. 2022;11(9). doi:10.3390/cells11091464
24. He J, Zhang N, Zhu Y, Jin R, Wu F. MSC spheroids-loaded collagen hydrogels simultaneously promote neuronal differentiation and suppress inflammatory reaction through PI3K-Akt signaling pathway. *Biomaterials*. 2021;265:120448. doi:10.1016/j.biomaterials.2020.120448
25. Mathot F, Shin AY, Van Wijnen AJ. Targeted stimulation of MSCs in peripheral nerve repair. *Gene*. 2019;710:17–23. doi:10.1016/j.gene.2019.02.078
26. Li X, Guan Y, Li C, et al. Immunomodulatory effects of mesenchymal stem cells in peripheral nerve injury. *Stem Cell Res Ther*. 2022;13(1):18. doi:10.1186/s13287-021-02690-2
27. Bow A, Newby S, Rifkin R, et al. Evaluation of a polyurethane platform for delivery of nanohydroxyapatite and decellularized bone particles in a porous three-dimensional scaffold. *ACS Appl Bio Mater*. 2019;2(5):1815–1829. doi:10.1021/acsabm.8b00670
28. Newby SD, Masi T, Griffin CD, et al. Functionalized graphene nanoparticles induce human mesenchymal stem cells to express distinct extracellular matrix proteins mediating osteogenesis. *Int J Nanomed*. 2020;15:2501–2513. doi:10.2147/IJN.S245801
29. Macdonald AF, Trotter RD, Griffin CD, et al. Genetic profiling of human bone marrow and adipose tissue-derived mesenchymal stem cells reveals differences in osteogenic signaling mediated by graphene. *J Nanobiotechnol*. 2021;19(1). doi:10.1186/s12951-021-01024-x
30. Alghazali KM, Newby SD, Nima ZA, et al. Functionalized gold nanorod nanocomposite system to modulate differentiation of human mesenchymal stem cells into neural-like progenitors. *Sci Rep*. 2017;7(1):16654. doi:10.1038/s41598-017-16800-9
31. Pedersen A. *Biomaterials for Soft Tissue Applications*. Knoxville: The University of Tennessee; 2021.
32. Harley-Troxell ME, Dhar M. Assembling spheroids of rat primary neurons using a stress-free 3D culture system. *Int J Mol Sci*. 2023;24(17). doi:10.3390/ijms241713506
33. Ghosh Dastidar A, Clarke SA, Larraneta E, Buchanan F, Manda K. In vitro degradation of 3D-Printed Poly(L-lactide-Co-Glycolic Acid) scaffolds for tissue engineering applications. *Polymers*. 2023;15(18). doi:10.3390/polym15183714
34. Wu H, Wei X, Liu Y, et al. Dynamic degradation patterns of porous polycaprolactone/beta-tricalcium phosphate composites orchestrate macrophage responses and immunoregulatory bone regeneration. *Bioact Mater*. 2023;21:595–611. doi:10.1016/j.bioactmat.2022.07.032
35. Zhao YN, Wu P, Zhao ZY, et al. Electrodeposition of chitosan/graphene oxide conduit to enhance peripheral nerve regeneration. *Neural Regen Res*. 2023;18(1):207–212. doi:10.4103/1673-5374.344836
36. Wachs RA, Wellman SM, Porvasnik SL, et al. Apoptosis-decellularized peripheral nerve scaffold allows regeneration across nerve gap. *Cells Tissues Organs*. 2022:1–11. doi:10.1159/000525704
37. Li C, Zhang M, Liu SY, et al. Chitin nerve conduits with three-dimensional spheroids of mesenchymal stem cells from SD rats promote peripheral nerve regeneration. *Polymers*. 2021;13(22). doi:10.3390/polym13223957
38. Wu W, Dong Y, Liu H, et al. 3D printed elastic hydrogel conduits with 7,8-dihydroxyflavone release for peripheral nerve repair. *Mater Today Bio*. 2023;20:100652. doi:10.1016/j.mtbio.2023.100652
39. Li A, Pereira C, Hill EE, Vukcevich O, Wang A. In vitro, in vivo and ex vivo models for peripheral nerve injury and regeneration. *Curr Neuropharmacol*. 2022;20(2):344–361. doi:10.2174/1570159X19666210407155543
40. Harley-Troxell ME, Steiner R, Newby SD, et al. Electro-spun PCL nerve wrap coated with graphene oxide supports axonal growth in a rat sciatic nerve injury model. *Pharmaceutics*. 2024;16(10):1254.

41. Steiner R, Dhar M, Stephenson SM, et al. Biometric data comparison between Lewis and Sprague Dawley rats. *Front Vet Sci*. 2019;6:469. doi:10.3389/fvets.2019.00469
42. Lakes EH, Allen KD. Gait analysis methods for rodent models of arthritic disorders: reviews and recommendations. *Osteoarthritis Cartilage*. 2016;24(11):1837–1849. doi:10.1016/j.joca.2016.03.008
43. Chen K, Xu M, Ren Y, et al. Preparation of magnetic graphene nanocomposites for fast detection of nitrobenzene in environmental water samples by GC–MS. *Chromatographia*. 2014;78(1–2):131–137. doi:10.1007/s10337-014-2815-5
44. El Kelany R, Moustafa K, El Mehy G. Titanium-induced histological and immunohistochemical alterations in liver, spleen, lung and kidney in male albino rats. *Ain Shams J Forensic Med Clin Toxicol*. 2013;20(1):146–157. doi:10.21608/ajfm.2013.19400
45. Malatesta M. Transmission electron microscopy as a powerful tool to investigate the interaction of nanoparticles with subcellular structures. *Int J Mol Sci*. 2021;22(23). doi:10.3390/ijms222312789
46. Badia J, Pascual-Font A, Vivo M, Udina E, Navarro X. Topographical distribution of motor fascicles in the sciatic-tibial nerve of the rat. *Muscle Nerve*. 2010;42(2):192–201. doi:10.1002/mus.21652
47. Tijs C, van Dieen JH, Baan GC, Maas H. Three-dimensional ankle moments and nonlinear summation of rat triceps surae muscles. *PLoS One*. 2014;9(10):e111595. doi:10.1371/journal.pone.0111595
48. Isaacs J, Mallu S, Wo Y, Shah S. A rodent model of partial muscle re-innervation. *J Neurosci Methods*. 2013;219(1):183–187. doi:10.1016/j.jneumeth.2013.07.019
49. Ouyang L, Zhang F, Liu J, et al. Application of oblique nerve coaptation in autologous nerve transplantation. *Ann Transl Med*. 2020;8(20):1300. doi:10.21037/atm-20-6526
50. Zhou S, Wu M, Chen G, et al. Effects of repeated transection and coaptation of peripheral nerves on axonal regeneration and motoneuron survival. *J Plast Reconstr Aesthet Surg*. 2019;72(8):1326–1333. doi:10.1016/j.bjps.2019.03.034
51. Lin J, Shi J, Min X, et al. The GDF11 promotes nerve regeneration after sciatic nerve injury in adult rats by promoting axon growth and inhibiting neuronal apoptosis. *Front Bioeng Biotechnol*. 2021;9:803052. doi:10.3389/fbioe.2021.803052
52. MacDonald AF, Harley-Troxell ME, Newby SD, Dhar MS. 3D-printing graphene scaffolds for bone tissue engineering. *Pharmaceutics*. 2022;14(9):1834. doi:10.3390/pharmaceutics14091834
53. Yunus MA, Ramli MM, Osman NH, Mohamed R. Stimulation of innate and adaptive immune cells with graphene oxide and reduced graphene oxide affect cancer progression. *Arch Immunol Ther Exp*. 2021;69(1):20. doi:10.1007/s00005-021-00625-6
54. Dudek I, Skoda M, Jarosz A, Szukiewicz D. The molecular influence of graphene and graphene oxide on the immune system under in vitro and in vivo conditions. *Arch Immunol Ther Exp*. 2016;64(3):195–215. doi:10.1007/s00005-015-0369-3
55. Mohammadinejad R, Moosavi MA, Tavakol S, et al. Necrotic, apoptotic and autophagic cell fates triggered by nanoparticles. *Autophagy*. 2019;15(1):4–33. doi:10.1080/15548627.2018.1509171
56. Dabrowski B, Zuchowska A, Brzozka Z. Graphene oxide internalization into mammalian cells - a review. *Colloids Surf B Biointerfaces*. 2023;221:112998. doi:10.1016/j.colsurfb.2022.112998
57. Lawkowska K, Pokrywczynska M, Koper K, Kluth LA, Drewa T, Adamowicz J. Application of graphene in tissue engineering of the nervous system. *Int J Mol Sci*. 2021;23(1). doi:10.3390/ijms23010033
58. Tang M, Song Q, Li N, Jiang Z, Huang R, Cheng G. Enhancement of electrical signaling in neural networks on graphene films. *Biomaterials*. 2013;34(27):6402–6411. doi:10.1016/j.biomaterials.2013.05.024
59. Tupone MG, Panella G, d'Angelo M, et al. An update on graphene-based nanomaterials for neural growth and central nervous system regeneration. *Int J Mol Sci*. 2021;22(23). doi:10.3390/ijms222313047
60. Webb K, Hlady V, Tresco PA. Relationships among cell attachment, spreading, cytoskeletal organization, and migration rate for Anchorage-dependent cells on model surfaces. *J Biomed Mater Res*. 2000;49(3):362–368.
61. Xia J, Liu ZY, Han ZY, et al. Regulation of cell attachment, spreading, and migration by hydrogel substrates with independently tunable mesh size. *Acta Biomater*. 2022;141:178–189. doi:10.1016/j.actbio.2022.01.025
62. Makadia HK, Siegel SJ. Poly Lactic-co-Glycolic Acid (PLGA) as biodegradable controlled drug delivery carrier. *Polymers*. 2011;3(3):1377–1397. doi:10.3390/polym3031377
63. Hussein AS, Abdullah N, Ahmadun FR. In vitro degradation of poly (D, L-lactide-co-glycolide) nanoparticles loaded with linamarin. *IET Nanobiotechnol*. 2013;7(2):33–41. doi:10.1049/iet-nbt.2012.0012
64. Raslan A, Saenz Del Burgo L, Ciriza J, Pedraz JL. Graphene oxide and reduced graphene oxide-based scaffolds in regenerative medicine. *Int J Pharm*. 2020;580:119226. doi:10.1016/j.ijpharm.2020.119226
65. Convertino D, Trincavelli ML, Giacomelli C, Marchetti L, Coletti C. Graphene-based nanomaterials for peripheral nerve regeneration. *Front Bioeng Biotechnol*. 2023;11:1306184. doi:10.3389/fbioe.2023.1306184
66. Committee MUAC. Laboratory animal biomethodology workshop. Comparative Medicine Animal Resource Center; 2020.
67. Ema M, Gamo M, Honda K. A review of toxicity studies on graphene-based nanomaterials in laboratory animals. *Regul Toxicol Pharmacol*. 2017;85:7–24. doi:10.1016/j.yrtph.2017.01.011
68. Tabish TA, Pranjol MZI, Jabeen F, et al. Investigation into the toxic effects of graphene nanopores on lung cancer cells and biological tissues. *Appl Mater Today*. 2018;12:389–401. doi:10.1016/j.apmt.2018.07.005
69. Wen KP, Chen YC, Chuang CH, Chang HY, Lee CY, Tai NH. Accumulation and toxicity of intravenously-injected functionalized graphene oxide in mice. *J Appl Toxicol*. 2015;35(10):1211–1218. doi:10.1002/jat.3187
70. Zheng S, Wei H, Cheng H, et al. Advances in nerve guidance conduits for peripheral nerve repair and regeneration. *Am J Stem Cells*. 2023;12(5):112–123.
71. Liu B, Xin W, Tan JR, et al. Myelin sheath structure and regeneration in peripheral nerve injury repair. *Proc Natl Acad Sci U S A*. 2019;116(44):22347–22352. doi:10.1073/pnas.1910292116
72. Latremoliere A, Cheng L, DeLisle M, et al. Neuronal-specific TUBB3 is not required for normal neuronal function but is essential for timely axon regeneration. *Cell Rep*. 2018;24(7):1865–1879e9. doi:10.1016/j.celrep.2018.07.029
73. Choe MA, Kim KH, An GJ, Lee KS, Heitkemper M. Hindlimb muscle atrophy occurs from peripheral nerve damage in a rat neuropathic pain model. *Biol Res Nurs*. 2011;13(1):44–54. doi:10.1177/1099800410382291

74. Fukutani A, Hashizume S, Isaka T. Measurements of tendon length changes during stretch-shortening cycles in rat soleus. *Sci Rep*. 2023;13 (1):5381. doi:10.1038/s41598-023-32370-5
75. Rivares C, Brunner R, Pel JJM, Baan GC, Huijing PA, Jaspers RT. Remodeling of Rat M. Gastrocnemius medialis during recovery from aponeurotomy. *Front Physiol*. 2020;11:541302. doi:10.3389/fphys.2020.541302
76. Faustino-Rocha AI, Oliveira PA, Duarte JA, Ferreira R, Ginja M. Ultrasonographic evaluation of gastrocnemius muscle in a rat model of N-Methyl-N-nitrosourea-induced Mammary Tumor. *in vivo*. 2013;3(27):803–808.